Earth and Planetary Science Letters 439 (2016) 109–116

Contents lists available at ScienceDirect

Earth and Planetary Science Letters

www.elsevier.com/locate/epsl

Constraints on accumulated strain near the ETS zone along Cascadia

Randy D. Krogstad [a,*], David A. Schmidt [b], Ray J. Weldon [a], Reed J. Burgette [c]

[a] Department of Geological Sciences, University of Oregon, United States
[b] Department of Earth and Space Sciences, University of Washington, United States
[c] Department of Geological Sciences, New Mexico State University, United States

ARTICLE INFO

Article history:
Received 6 November 2015
Received in revised form 21 January 2016
Accepted 24 January 2016
Available online 8 February 2016
Editor: P. Shearer

Keywords:
slow slip
episodic tremor and slip
Cascadia
subduction zone
strain accumulation
surface deformation

ABSTRACT

Current national seismic hazard models for Cascadia use the zone of episodic tremor and slip (ETS) to denote the lower boundary of the seismogenic zone. Recent numerical models have suggested that an appreciable amount of long-term strain may accumulate at the depth of ETS and questions this assumption. We use uplift rates from leveling campaigns spanning approximately 50–70 yrs in Washington and Oregon to investigate the amount of potential long-term locking near the ETS zone. We evaluate the potential for deeper locking in Cascadia by exploring a range of locking parameters along the subduction zone, including the ETS zone. Of the four east–west leveling profiles studied, three show a reduction in the misfit when secondary locking near the ETS zone is included; however the reduction in misfit values is only statistically significant for one profile. This would suggest that models including a small amount of secondary locking are broadly indistinguishable from models without any secondary locking. If secondary locking is considered, the leveling data allow for locking up to ~20% of the plate rate near the updip edge of the ETS zone. These results are consistent with, but less resolved, by GPS observations.

1. Introduction

The Cascadia subduction zone poses a significant seismic hazard to the Pacific Northwest due to the potential of a megathrust earthquake (Atwater, 1987; Goldfinger et al., 2003). Geodetic and thermal data suggest that strain is actively accumulating along the plate boundary (Hyndman and Wang, 1995). Seismic hazard maps that quantify the expected strong motion from a megathrust event are constructed from a logic tree of rupture scenarios. One branch of these rupture scenarios implicitly assumes that seismic rupture will not extend into the zone of episodic tremor and slip (ETS) (Peterson et al., 2014). Considering the importance that this assumption has on the seismic hazard, we explore the potential for long-term strain accumulation near the ETS zone.

In Cascadia, ETS events represent the transient release of accumulated strain along the plate interface downdip from the seismogenically locked zone at 25–45 km depth. These ~M_w 6 ETS events last approximately 10–20 days and have recurrence intervals of 11–22 months (Dragert et al., 2001; Rogers and Dragert, 2003; Brudzinski and Allen, 2007; Schmidt and Gao, 2010). The existence of ETS demonstrates that the subducting and overriding plates are capable of storing strain at this depth for months to years, and perhaps longer. The limited resolution of slip on the deep part of the plate interface leaves considerable uncertainty as to whether any strain might accumulate over multiple ETS cycles near the ETS zone, thereby potentially elevating the seismic hazard by increasing the down-dip limit of the seismogenic locked zone and extending the rupture zone inland toward large population centers.

Geodetic inversions of major slow slip events (SSEs) in northwest Washington from 1997–2008 reveal that only 50–60% of the long-term strain accumulation is released at 25–45 km depth (Chapman and Melbourne, 2009; Schmidt and Gao, 2010). Smaller SSEs, which are difficult to resolve geodetically, may account for the remaining slip deficit within the ETS zone. Based on tremor that accompanies slow slip, Wech et al. (2009) inferred that up to 45% of the strain budget might be attributed to background activity in the inter-ETS interval. This would suggest that nearly the entire strain budget that is accumulated around the plate boundary within the depth interval of ~25–45 km is released in ETS activity. In contrast, rate-and-state numerical models of SSEs have predicted that a sizable portion (~30–50%) of the slip deficit remains after multiple events (Segall et al., 2010; Colella et al., 2013).

In this work, we investigate the presence of elastic strain that is accumulated within the depth range of 25–45 km on the plate

* Corresponding author at: Department of Geological Sciences, University of Oregon, Eugene, OR 97403, USA.
E-mail address: krogstad@uoregon.edu (R.D. Krogstad).

http://dx.doi.org/10.1016/j.epsl.2016.01.033

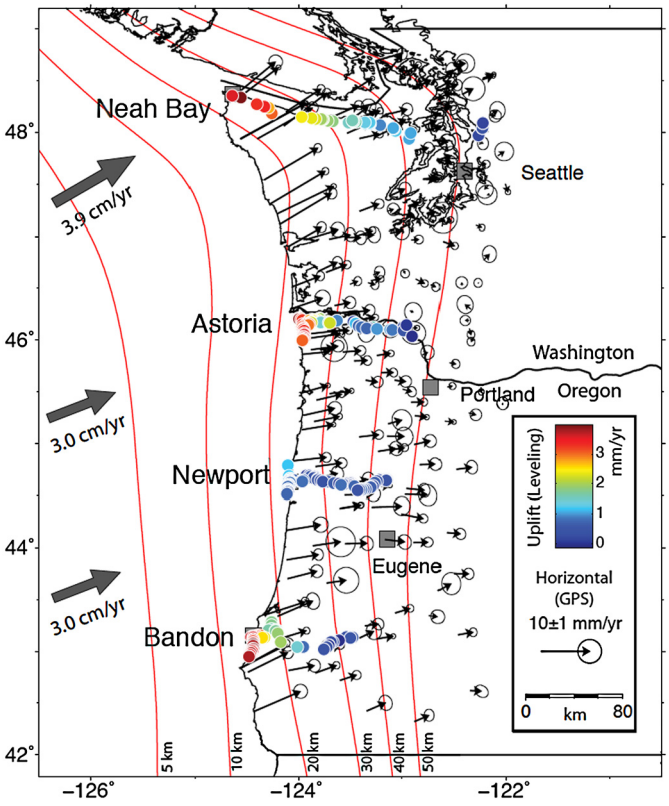

Fig. 1. Vertical and horizontal velocities in Cascadia used in this study. Colored dots represent absolute uplift rates from the four east–west trending leveling profiles. Black arrows represent horizontal velocities from permanent and campaign GPS measurements. GPS velocities are relative to North America and have been corrected for the Oregon block rotation. Error ellipses are 95% confidence. Red contour lines are depths of the subducting Juan de Fuca plate beneath North America from McCrory et al. (2004). Grey arrows indicate the Juan de Fuca to fore-arc convergence rates. (For interpretation of the references to color in this figure legend, the reader is referred to the web version of this article.)

boundary and released during a typical megathrust cycle through the optimization of locking parameters. Although the kinematic behavior of ETS has predominately been characterized using geodetic (i.e. GPS and strain gauges) and seismic measurements (i.e. tremor) from the last 1–2 decades, historical leveling and tide gauge data, which extend back nearly 8 decades, provide a means to supplement and extend these recent observations to gain a better understanding of long-term deformation in the ETS zone. When tied to an absolute reference frame with tide gauge data, leveling data provide precise uplift measurements with uncertainties significantly lower than current vertical GPS measurements. Our findings suggest that the long term accumulated strain is less than predicted by some numerical models, but the data do allow for a small portion of the slip budget to be stored over multiple ETS cycles.

2. Data and methodology

For this study, the vertical displacements of four east–west leveling profiles along Cascadia are analyzed: three in Oregon (Burgette et al., 2009), and one in northern Washington reprocessed with a similar methodology (Fig. 1; Supplementary Text S1). Relative uplift rates are derived from National Geodetic Survey (NGS) first- and second-order leveling surveys along highways in western Oregon and Washington, spanning a time-scale from the early 1930s to the late 1980s. Burgette et al. (2009) estimated up to 80 years worth of uplift rates along the surveys in Cascadia by making secondary ties to benchmarks, correcting for sea level rise rates, and improving the data processing.

Each leveling profile is tied to benchmarks at tide gauge stations. After accounting for regional sea level rise, the tide gauge uplift rates are used to provide an absolute reference frame to the relative uplift rates from the leveling profiles. This, along with additional processing methods, helps to significantly reduce the standard error of benchmark uplift rates to $\sim$0.3 mm a^{-1} along the coast, with the error increasing to the east away from the tide gauge benchmarks to $\sim$1 mm a^{-1}. Refer to Burgette et al. (2009) and the supplement for the complete details of the processing procedure. We have greater trust in data points with higher uplift rates, since individual benchmarks tend to subside over time and can be biased downward. However, all reported data are used in our analysis.

To complement the leveling results we also include an analysis of GPS displacements near the leveling profiles. Due to higher uncertainties and scatter in the vertical component of GPS compared to our leveling data set, we choose to only use the horizontal GPS components. We use network site velocities in Cascadia from continuous and campaign GPS observations compiled, analyzed, and made available by McCaffrey et al. (2013), which includes data from the Plate Boundary Observatory, Pacific Northwest Geodetic Array, Western Canada Deformation Array, National Geodetic Survey Continuously Operating Reference Sites, and several others. The velocities are restricted to sites with at least five years of data, and are spatially binned to coincide with the leveling profiles. Sites near major volcanic centers are removed. The rotation of Oregon and southern Washington is removed using the pole and rate of rotation derived by McCaffrey et al. (2013). The north and east oriented velocity vectors are rotated into convergence normal and convergence parallel components. This allows us to focus on the convergence parallel component, where the maximum deformation signal is observed.

Time-dependent deformation along the fault since the last major rupture (i.e. viscous relaxation of the lower crust or upper mantle) could affect the GPS and leveling data differently. Considering our model assumes an isotropic elastic medium, we do not explore how the deformation might evolve with time. Due to the difference in averaging intervals and the relative difficulty of resolving the expected signal due to secondary locking in horizontal displacements (Fig. 2) the leveling and GPS datasets are analyzed individually.

To model the subduction zone, a backslip method is used to estimate the slip deficit on the subduction interface (Savage et al., 2000). The convergence rate is calculated using the Juan de Fuca–Oregon forearc Euler pole of Wells and Simpson (2001) for the Oregon profiles and the Juan de Fuca–North America pole of Mazzotti et al. (2007) for the Washington profile. The Juan de Fuca slab interface is modeled by discretizing the depth contours of McCrory et al. (2004) into triangular subfault patches. Surface deformation is estimated using an isotropic elastic half space with a Poisson's ratio of 0.25 and a shear modulus of 40 GPa. Green's functions are calculated using the boundary element program Poly3D (Thomas, 1993). Slip is ascribed using a combination of dip-slip and strike-slip motion to account for oblique convergence of the Juan de Fuca plate with North America. The slip deficit along the plate interface is prescribed by four free parameters: the down-dip extent of the primary seismogenic zone (locked zone), the down-dip extent of the transition zone, and a zone of partial locking near the ETS zone (also referred to as the zone of secondary locking) where the location and magnitude of the locking are allowed to vary separately.

The slip deficit rate in the seismogenically locked zone is assumed to be the full convergence rate and fully locked to the trench. Although this assumption may not hold true, our model re-

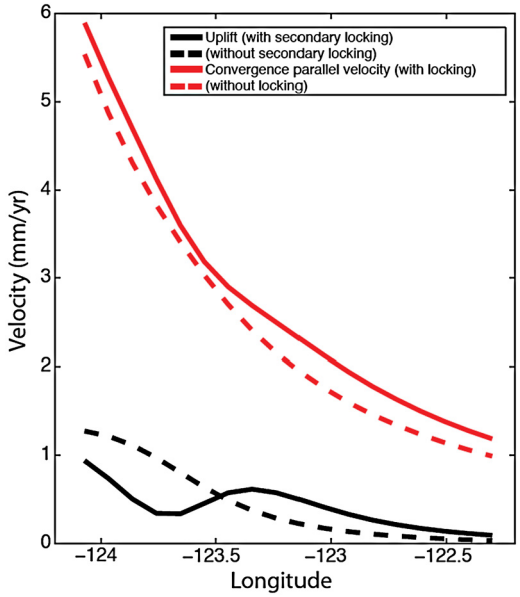

Fig. 2. Expected displacement rates in central Oregon for vertical and convergence parallel deformation. Solid lines and dashed lines depict the expected velocities with and without including partial locking near the ETS zone, respectively. The depth of the locked and transitions zones are the same. The model including locking has 15% locking at a depth of 33 km. The expected signal in the vertical component is more distinctive than that expressed in the horizontal component of surface velocity.

sults are insensitive to the extent of locking near the trench given that all of our observations are onshore. In the transition zone, the slip deficit rate decays exponentially from the full convergence rate to zero as described by Wang et al. (2003). We parameterize the slip deficit function near the ETS zone as a Gaussian distribution of partial locking with a 1-sigma along-dip width of 2 km. The magnitude of coupling and the location of the peak of the Gaussian are allowed to vary. This distribution of strain accumulation was chosen to correspond with the general shape of observed tremor density (Wech and Creager, 2011). A sensitivity analysis revealed that the model results for depth and magnitude of the secondary coupling are relatively insensitive to the prescribed shape (i.e. triangular, Gaussian, or boxcar).

An iterative procedure is run to explore the full model parameter space. We consider locked zone depths ranging from 5 to 25 km, transition zone depths of 10–40 km, peak ETS zone locking depths of 25–40 km, and peak ETS zone locking of 0–40%. We forward predict the surface displacements and evaluate the goodness of fit by calculating the weighted root mean square (WRMS) using the data uncertainties for each iteration of the model parameters (Fig. 3). Misfit plots show the WRMS as a function of the model parameters (Fig. 4). Given that a range of model parameters produce a low WRMS, we use a t-test and consider all models within a 70% confidence interval from the model that produces the minimum WRMS to be statistically indistinguishable. Additionally, we consider models that both include and exclude a zone of secondary locking; an F-test is used to evaluate whether the increase in model parameters provides a statistically significant improvement in the WRMS values.

The WRMS approach assumes that the leveling data is composed of independent observations. However, leveling data is known to contain spatially correlated errors that propagate along leveling lines. To compare the effects of different error models, we also use the approach described in Pollitz et al. (1998) where the covariance matrix is formulated as a combination of measurement and non-measurement error. Measurement error is correlated and dependent on the distance between neighboring benchmarks, while non-measurement errors are uncorrelated and can come from many different sources (e.g. soil compaction) (Amoruso and Crescentini, 2007). The measurement error is accounted for using the method of Arnadottir et al. (1992) where the covariance matrix is of a form that treats the differences of the benchmark-to-benchmark heights as being measured directly. This allows for the data to be treated as independent and uncorrelated. This approach strongly weights spatially clustered benchmarks and is particularly sensitive to steep localized gradients in the uplift profile. To account for the non-measurement error, Pollitz et al. (1998) include an additional general error term of 0.5 mm/yr that is meant to account for the long-period noise levels found in vertical measurements, as described by Wyatt (1989). From this, we construct a covariance matrix that includes off-diagonal terms in the weighting matrix. The results of these two error model approaches are compared in the following section.

3. Results

3.1. Leveling analysis

The Neah Bay, Astoria, and Newport profiles all exhibit a reduction in the WRMS when a secondary locked zone is included near the ETS zone. However, the Newport profile is the only one that provides a statistically significant improvement in WRMS values. The leveling data extending from Bandon, Oregon is the only profile that is best fit without secondary locking. Based on the 70% confidence interval limit for acceptable models described in the methods section, acceptable models show a maximum secondary locking in the range of 10–20% (Fig. 4).

The best-fit models for the Neah Bay profile have a peak locking of ∼5% located at 33–35 km depth (Figs. 3 and 4). The eastern side of the northern Washington leveling profile has a gap where it crosses Puget Sound. The points directly west of the Puget Sound gap (longitude of ~ -123) show a subtle leveling-off of uplift rates, which diverges from the linear eastward trend in decreasing uplift rates observed in the western portion of the profile. A model that includes locking in the ETS zone better fits these points on the western edge of Puget Sound, but the lack of data within the Sound makes quantifying the precise magnitude of the locking difficult.

The best-fit models for Astoria have a peak secondary locking of 5–15% located at 28–33 km depth. The high uplift values at ∼123.2 degrees are under-fit by these models because of the significantly more abundant data points on the western end of the profile (Figs. 3 and 4). We can improve the fit of the data on the eastern end of the profile by manually shifting the peak of the coupling in the ETS zone to 34 km depth and increasing the locking to 20% at a cost of ∼9% increase in the overall WRMS for the entire dataset.

The Newport profile is statistically better fit when locking near the ETS zone is included, as indicated by an F-test. The secondary uplift is very distinct, and the relatively more dense data sampling on the eastern end of the profile compared to other profiles allows us to better constrain the locking near the ETS zone. The diminished coastal uplift suggests that the locked zone is far offshore, or is only partially locked. This leads to uncertainty in the amount of locking in the primary locked zone, as evidenced by the relatively broad misfit field in Fig. 4. Deceasing the locking in the seismogenically locked zone to 50% would extend the locked zone to a depth of 16 km and would be accompanied by a similar transition zone depth of 30 km. Regardless of how locking is assigned in the primary locked zone, the secondary uplift signature is still best fit with secondary locking at approximately 32–35 km depth with 15–25% locking.

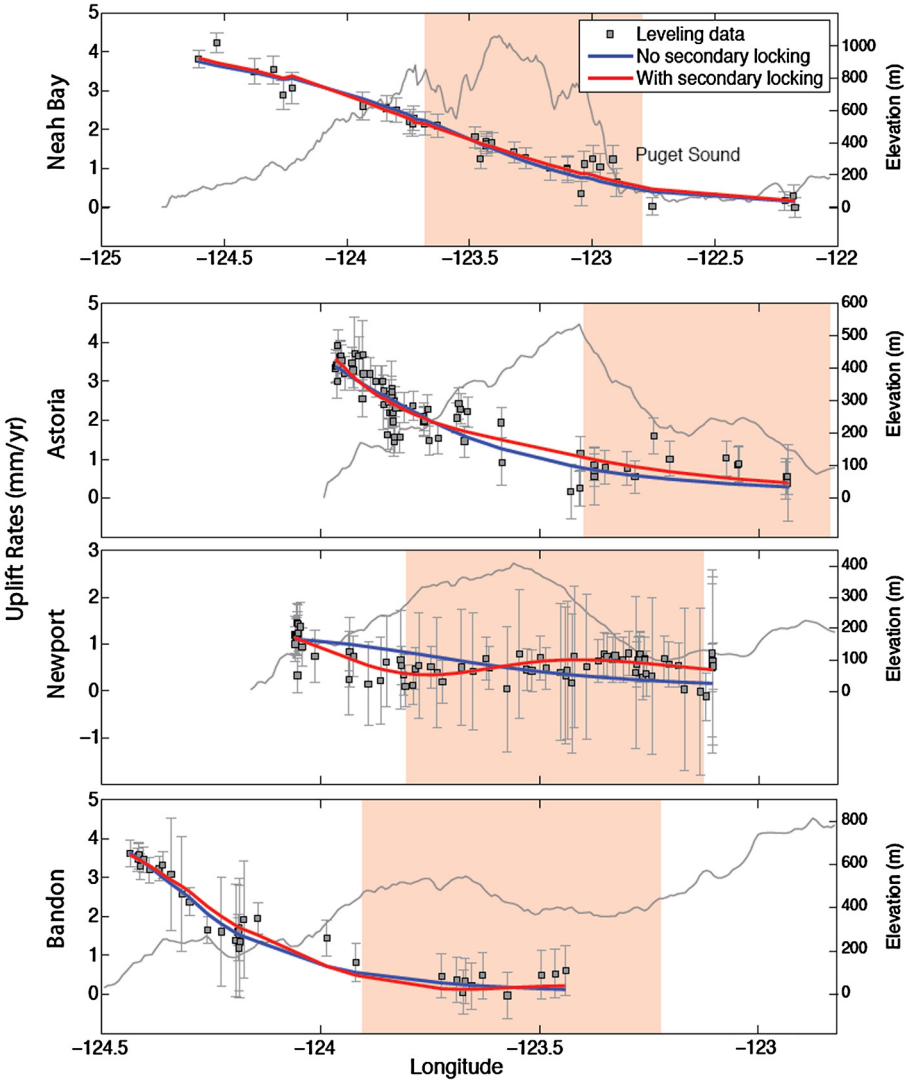

Fig. 3. Observed and modeled uplift rates along Cascadia. Red and blue lines indicate the best-fit modeled uplift rates at each leveling benchmark with and without including locking near the ETS zone respectively. Error bars are one sigma. Grey lines are the average topography in the region of the leveling profiles. Pink shaded regions indicate the longitudinal distribution of tremor along the leveling profiles. (For interpretation of the references to color in this figure legend, the reader is referred to the web version of this article.)

The Bandon profile is best fit with little to no locking near the ETS zone. However, the eastern most extent of the Bandon profile ends in the region where the secondary uplift is observed in the other two Oregon profiles. The easternmost points on the profile show an increasing uplift trend. Since these few points have a minimal impact on the overall fit of the profile, the optimized parameters do not adequately fit these eastern points. When a forward model is forced to fit the eastern most points, the results indicate secondary locking at 28–32 km depth with 5–10% locking, although this leads to some systematic misfits of the data directly west of the secondary uplift. This procedure raises the WRMS by ∼9% compared to the optimal model with no coupling. Alternatively, increasing the locking gradient of the transition zone can better fit the eastern data without adversely affecting the fit of the western data. While models with steep transition zones result in similar locked zone and secondary locking depths, the transition zone extends significantly deeper to ∼30–35 km.

The results using the full covariance matrix (Table S1 and Fig. S1) provide a close match with the results assuming independent data for each benchmark. We find that the differences between the two sets of model results are insignificant at the 90% confidence interval for all of the profiles except Bandon. The Astoria profile has the largest difference in optimal secondary locking values, with an increase of 15% when using the full covariance matrix. Additionally, the best-fit locked and transition zone depths for Astoria are likely physically unrealistic, with both being located at 21 km. This method works well for leveling profiles that have approximately evenly spaced benchmarks such as the Neah Bay and Newport profiles. However, the Astoria and Bandon profiles have many closely spaced benchmarks near the coast and relatively few distantly spaced benchmarks extending inland, which results in a much lower weighting of the eastern most data where the largest signal from the secondary locking would be expected. Thus the heterogeneous sampling along the Astoria profile may explain why the results differ between the two weighting schemes. The optimization using the full covariance is also more sensitive to outliers that create steep gradients in the uplift profile. All of the Cascadia profiles contain outliers that are likely due to localized non-tectonic subsidence, which affect the overall fit to varying degrees depending on the location of the neighboring benchmarks. Although this approach better accounts for the correlated nature of leveling data and is suitable for profiles such as Neah Bay and Newport, we have found that it may not be appropriate for char-

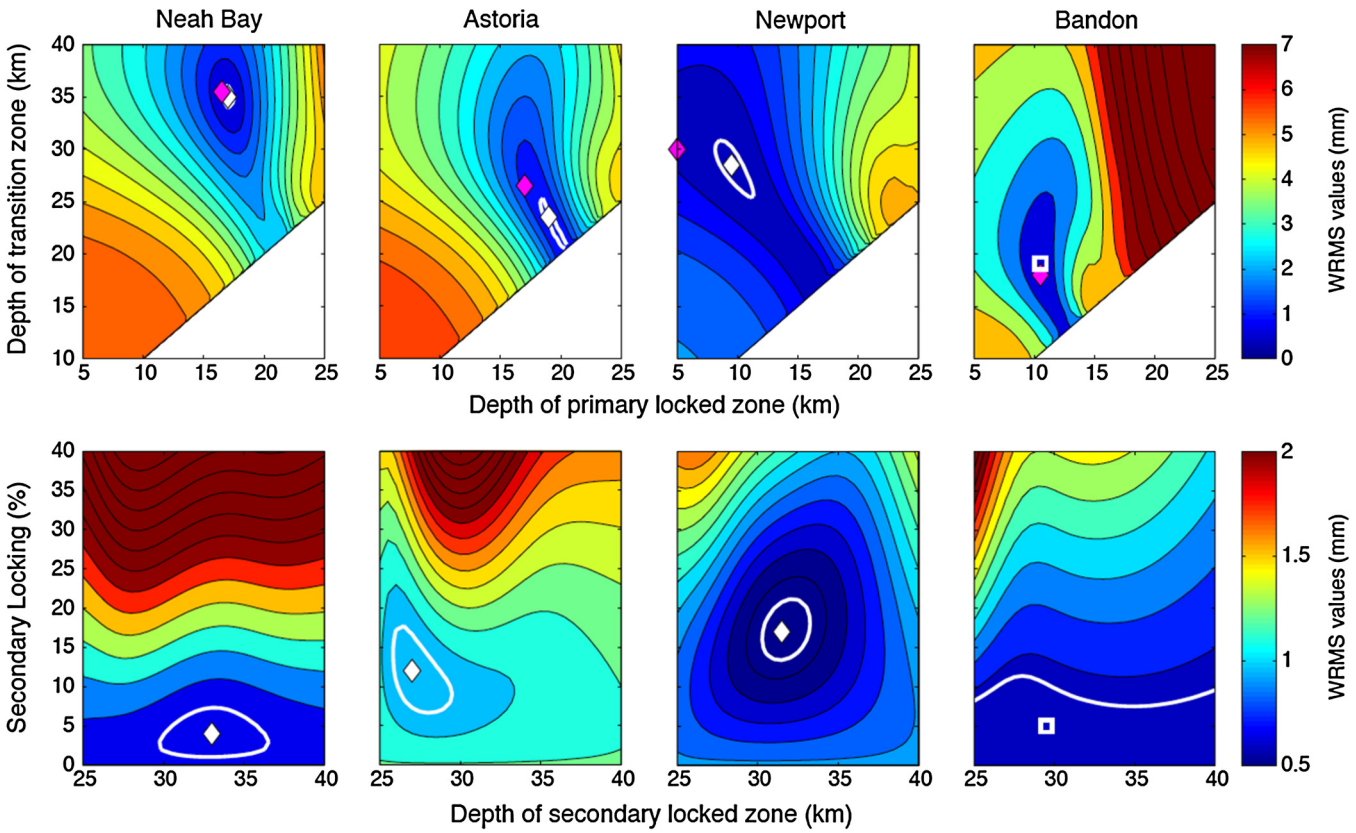

Fig. 4. Weighted root mean square (WRMS) misfit plotted as a function of model parameters for all four leveling profiles. (a) Depths of the locked zone and transition zone. White areas fall outside of the modeled parameter space. (b) Depth and magnitude of coupling near the ETS zone. White diamonds mark the optimal fit (lowest WRMS). The white squares on the Bandon plots represent the preferred fit to eastern most leveling benchmarks. Magenta diamonds in the upper panels mark the optimal fit of models without secondary locking. Acceptable models fall within the white contours, which encircle model parameters within the 70% confidence level of the minimum WRMS. (For interpretation of the references to color in this figure legend, the reader is referred to the web version of this article.)

Table 1
Optimal model fits of the leveling data with and without including locking near the ETS zone.

Leveling results	Neah Bay	Astoria	Newport	Bandon[a]
No locking in ETS zone				
Locked zone depth (km)	16.5	17	5[b]	10.5
Transition zone depth (km)	35.5	26.5	30	18
WRMS (mm/yr)	0.85	1.02	0.7	0.57
Including locking in ETS zone				
Locked zone depth (km)	17	19	9.5	10.5
Transition zone depth (km)	35	23.5	28.5	19
Optimal ETS zone locking (%)	4	12	17	5
Depth[c] of ETS zone locking (km)	33	27	31.5	29.5
WRMS (mm/yr)	0.8	0.96	0.41	0.62
Statistically significant[d] (90%)	No	No	Yes	NA

[a] The Bandon profile is better fit with no secondary locking. The secondary locking values are included to show that 5% secondary locking provides a statistically similar fit.
[b] Results are at the edge of the modeled parameter space.
[c] Midpoint depth of Gaussian slip distribution.
[d] Statistical significance is calculated using an F-test.

acterizing the secondary locking in the Astoria and Bandon profiles (see Table 1).

3.2. GPS analysis

The subtle change in the horizontal surface deformation due to a secondary locked zone makes detection difficult with current GPS data, when considering the signal-to-noise (Fig. 2). As can be seen with the Neah Bay profile in particular, a model containing a moderate (~10–15%) amount of coupling near the ETS zone does not provide a significantly different fit to the data (Table S2). For all the profiles, except Newport, the GPS results have a shallower seismogenically locked zone than the leveling results. This could, in part, be due to the fact that the GPS and leveling data are averaged over different time intervals, and are thus disproportionately affected by viscoelastic effects. The best-fit Newport and Bandon profiles have especially shallow locked zones, although models that have deeper locked zones and shallower transition zones can adequately fit the data as well (Figs. S2 and S3). The relatively short averaging interval of the GPS data, which covers a limited number of ETS cycles, might also affect the modeled long-term coupling in the ETS zone. For example, if a site velocity is derived using an averaging interval of 6 years and the ETS cycle is ~18 months the modeled results could show up to a 40% long-term strain accumulation in the ETS zone even if there is no long-term strain in that region. This likely explains why some GPS profiles have higher coupling ratios near the ETS zone compared to the leveling results. The location of the modeled peak coupling tends to match fairly well with the leveling results, although the coupling in the Neah Bay profile is best fit a few kilometers farther updip.

4. Discussion

We find supportive evidence for secondary locking along the Newport leveling profile. While the leveling profile near Bandon shows a small increase in WRMS values when secondary locking is included, the profiles near Neah Bay and Astoria show an overall improvement with the addition of secondary locking. For these three profiles, models with or without a small amount of secondary locking are statistically indistinguishable, and thus we

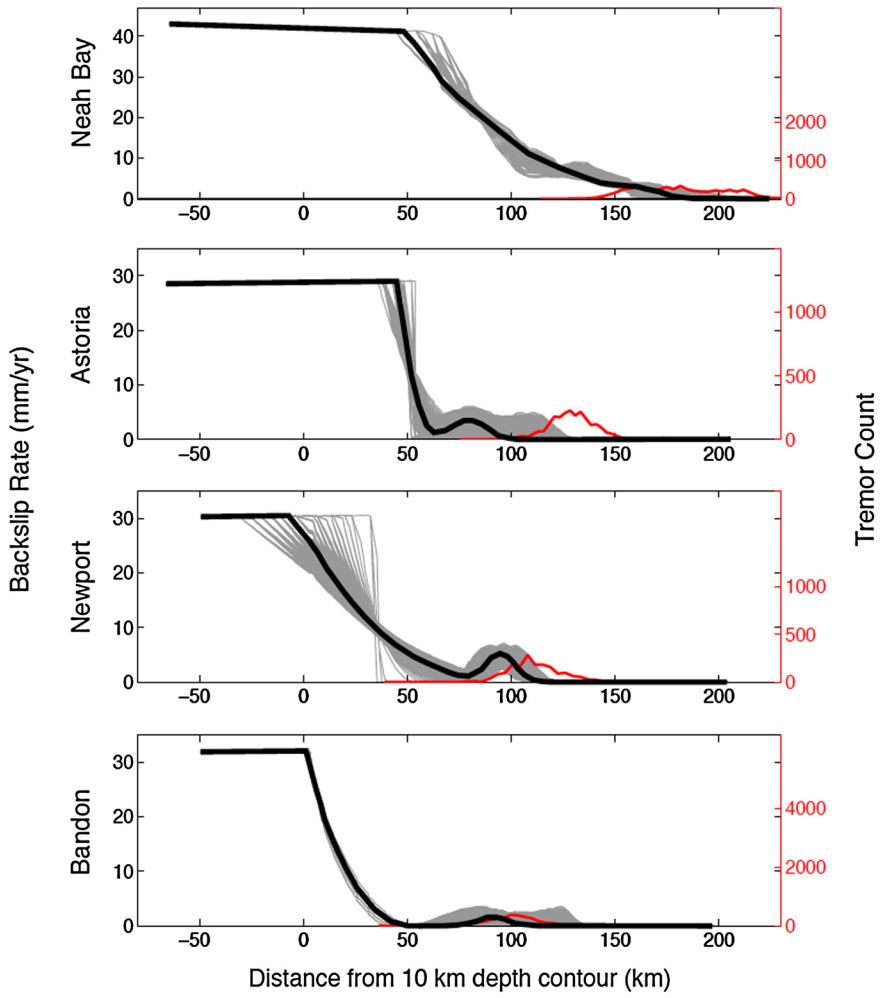

Fig. 5. Modeled backslip rates of the four leveling profiles in relation to tremor distribution assuming secondary locking. Black lines represent the modeled backslip along each leveling profile. Light grey lines represent the range in acceptable models within a 70% confidence interval (white contours in Fig. 4). Red lines are the distribution of tremor locations near each leveling profile. Tremor data is from the automated tremor catalog of Wech (2010) and spans Jan. 2010–Dec. 2013. The vertical axis of the tremor data (right axis) is scaled to compare the peak tremor with the locking in the ETS zone. The relatively broader tremor distribution along the Neah Bay profile is a combination of both the curved subduction zone and the actual tremor distribution. (For interpretation of the references to color in this figure legend, the reader is referred to the web version of this article.)

cannot rule out models with a limited amount of long-term strain accumulation near the ETS zone.

If long-term secondary locking exists within the ETS zone, our analysis suggests it is only a small fraction of the plate rate. The leveling data can be adequately fit with models that range from virtually no long-term locking, to models with an upper bound of about 20% of the plate rate. Chapman and Melbourne (2009) found that up to 15% percent locking might persist below 25 km depth when using the ETS zone to constrain the downdip extent of the transition zone in northern Washington. These results are compatible with the findings of Holtkamp and Brudzinski (2010) who analyzed long-term and transient signals in the GPS time-series. A few studies have also explored interseismic locking models with variable locking along dip, and they inferred a double locked zone, suggestive of a primary and secondary locked zone (McCaffrey et al., 2000; Verdonck, 2005). Thus, the existence of a secondary locked zone would be broadly consistent among these previous geodetic studies.

Secondary locking is expected to produce a broad, interior uplift signal, as illustrated by the forward model in Fig. 2. This interior uplift is most evident in the Newport leveling profile. However, the interior uplift may be difficult to identify in the other profiles either because it is masked by the primary locking signal from the seismogenic zone (i.e. Neah Bay profile), or because of insufficient data coverage to the east (i.e. Bandon profile). There are other possible explanations for this interior rise in the leveling data. It could represent a long wavelength artifact originating from the propagation of errors along the leveling line. Our error analysis is designed to compensate for this, as uncertainties increase along the leveling line and we explore the impact of spatially correlated data. We also see hints of an upward interior uplift for the Astoria profile, which should be independent from the Newport profile.

If we assume that 0–20% long-term strain is accumulating in the ETS zone, then we propose that this strain must be released at some point in the megathrust earthquake cycle. It is possible that this locking signal originates from some other tectonic process. For example, the underplating of sediment beneath the forearc, or vertical uplift by a buoyant mantle wedge could result in a subtle uplift of the forearc. However, these processes would produce long-term uplift that would result in elevated topography if the uplift persists over geological time scales. The broad uplift evident in the Newport profile is spatially offset from the topography of the coast range (Fig. 3). Thus, we conclude that the secondary strain accumulation, if present, must be an elastic process. What is unknown is when during the megathrust earthquake cycle this accumulated strain would be released, and whether it is released aseismically.

The small component of long-term locking modeled at all four profiles appears to be shifted relative to the peak tremor activity.

The approximate large-scale relationship between SSEs and tremor activity in Cascadia has been shown to correlate well both spatially and temporally, although inferences from geodetic observations in northern Washington tend to locate slip slightly updip of the peak tremor activity (e.g. Wang et al., 2008; Wech et al., 2009; Dragert and Wang, 2011; Bartlow et al., 2011). When the distribution of tremor is plotted with the modeled backslip profiles of the leveling data assuming secondary locking, the peak locking in the ETS zone is also located slightly updip of the peak tremor activity, placing the locking near the geodetically inferred slow slip (Fig. 5).

While there are tradeoffs in the locking parameters for the seismogenic zone, we find that the magnitude of the secondary locking in the ETS zone is generally insensitive to the amount of up-dip locking. McCaffrey et al. (2013) noted that it is possible to satisfy the surface deformation data in Oregon if maximum locking is reduced in the seismogenic zone. The assumption that the slip deficit rate in the seismogenically locked zone equals the full convergence rate does affect the depth of the locked zone and transition zone in our results. For example, the Astoria leveling profile can be fit reasonably well with levels of locking down to 70% on the updip portion of the interface, while the Newport profile can be reasonably fit with locking as low as 50% in the primary locked zone. However, the degree of locking in the seismogenic zone only has a minor effect on the amount of partial locking near the ETS zone. Additionally, the use of a heterogeneous elastic model, or a model that incorporates viscoelastic effects, may also help reduce the over WRMS values (Williams and Wallace, 2015; Wang et al., 2001). However, it is unlikely that the use of these models would affect the overall findings shown here.

One important additional relationship to note is that when the primary locked zone is assumed to be fully locked, models that include secondary locking tend to have modeled locked zones that are slightly deeper and shifted to the east. The difference in locked zone depths is typically only 1–2 km, but considering the seismic hazard imposed by the depth of the locked zone, this may be an important consideration for future seismic hazard maps.

A possible explanation for any residual strain accumulation in the ETS region is that the combination of large and inter-ETS SSEs, which are smaller ETS events not readily resolvable with geodetic methods, are not accommodating the total slip deficit of the subducting Juan de Fuca plate. While the combination of ETS and inter-ETS events is inferred to account for a nearly all of the remaining strain budget in this region (Ide et al., 2007; Aguiar et al., 2009), inter-ETS tremor is found downdip of regular ETS tremor (Wech et al., 2009; Wech and Creager, 2011), so may only accommodate the remaining slip deficit in the downdip portion of the ETS zone leaving a fraction of the slip deficit in the updip portion of the ETS zone.

The secondary locking along the subduction zone may be linked to the intersection of the Moho of the North American plate with the subducting plate interface. The physical and compositional changes near the Moho could result in an increase in locking by affecting several parameters, such as fluid migration from the dehydrating slab, a change in frictional stability, or a change in bulk strength of materials. In one possible explanation, which has also been proposed by Holtkamp and Brudzinski (2010), the increase in locking could be due to a rheological difference at the Moho, where the subducting slab encounters the stronger, potentially brittle, overriding mantle. Chen and Molnar (1983) showed that the composition of the upper mantle near the Moho allows for seismic deformation at higher temperatures (600 °C–800 °C) than the lithosphere (250 °C–450 °C). The area of secondary locking would then be constrained to the along-dip section of the plate boundary between the Moho and the high temperature onset of crystal plasticity in the mantle. The difference in temperatures at the Moho among subduction zones could help explain why different subduction zones exhibit different ETS behaviors.

Although there is some variability among studies, the Moho in Cascadia is typically thought to be at a depth of 30–40 km, with additional variability along strike (Bostock et al., 2002; Nedimovic et al., 2003; Nicholson et al., 2005; Wang et al., 2008; Peacock et al., 2011; Gao et al., 2011). This range in depth is consistent with the depth of tremor (Brown et al., 2009), as well as the modeled depth of the secondary locking found in the leveling data. The strength of the over-riding mantle would be at a maximum at the Moho and decrease with depth. This could explain why the modeled secondary locking, as well as geodetically derived slip distribution of SSEs, are located on the updip extent of the tremor distribution, while the inter-ETS tremor is located downdip of the peak secondary locking where the overriding mantle is weaker. Finer tomographic imaging of the Moho near the slab interface and more precise source locations of tremor may help to elucidate the spatial relationship of the mantle corner with ETS and the secondary locking.

While the model of Chen and Molnar (1983) provides a useful conceptual framework for understanding a region of locking in the ETS zone, we acknowledge that the fault interface is likely more complex than this simplified view. The fault zone is likely composed of heterogeneous materials that are sheared along the surface. The actual transition in fault properties and behaviors in this area is likely more diffuse. The overriding material along the fault in the ETS zone is thought to have low permeability which allows for elevated pore fluid pressures, decreasing the effective normal stress (Audet et al., 2009; Ghosh et al., 2010; Peacock et al., 2011). The ability to hold even a small amount of long-term strain in the ETS zone appears counter to the low effective stress that has been inferred for the ETS zone. A successful conceptual model must account for the how the fault is able to be temporarily weakened, while also maintaining partial long-term locking on the updip edge of the ETS zone that persists over many ETS cycles.

5. Conclusions

We have explored the potential of long-term strain accumulation near the ETS zone on Cascadia. Based on our findings, the assumption that ETS delineates the downdip extent of possible megathrust rupture may not be definite. However, we only have clear evidence of secondary locking from the Newport leveling profile. If locking exists near the ETS zone, it must be a small fraction of the plate rate. This small amount of partial locking is consistent with, but difficult to resolve in the GPS data, and may have significant implications on the kinematic behavior of the Cascadian subduction zone.

Secondary locking in the ETS zone must be released within the megathrust earthquake cycle. This could be accomplished by megathrust earthquakes propagating into the ETS zone, effectively extending the rupture area farther down-dip than previous models predict and increasing the moment magnitude by up to 5%. Alternatively, the accumulated strain could be released through aseismic processes, such as in future large ETS events, long-term ETS events, or as afterslip.

Acknowledgements

This work is supported by the U.S. Geological Survey (USGS), Department of the Interior, under USGS award number G11AP20062. Continuous GPS data used in this study are made available by the Plate Boundary Observatory (PBO) (http://pbo.unavco.org/) and the campaign GPS data comes from McCaffrey et al. (2013). The leveling and tide gauge data sets were collected and

made available by the National Oceanic and Atmospheric Administration (NOAA). Leveling data are accessed through the National Geodetic Survey [http://www.ngs.noaa.gov/] and the tide gauge data are accessible through the Center for Operational Oceanographic Products and Services (http://tidesandcurrents.noaa.gov/).

Appendix A. Supplementary material

Supplementary material related to this article can be found online at http://dx.doi.org/10.1016/j.epsl.2016.01.033.

References

Aguiar, A.C., Melbourne, T.I., Scrivner, C.W., 2009. Moment release rate of Cascadia tremor constrained by GPS. J. Geophys. Res. 114, B00A05. http://dx.doi.org/10.1029/2008JB005909.

Amoruso, A., Crescentini, L., 2007. Inversion of levelling data: how important is error treatment? Geophys. J. Int. 171 (3), 1352–1362. http://dx.doi.org/10.1111/j.1365-246X.2007.03585.x.

Arnadottir, T., Segall, P., Matthews, M., 1992. Resolving the discrepancy between geodetic and seismic fault models for the 1989 Loma Prieta, California earthquake. Bull. Seismol. Soc. Am. 82 (5), 2248–2255.

Atwater, B.F., 1987. Evidence for great Holocene earthquakes along the outer coast of Washington state. Science 236 (4804), 942–944. http://dx.doi.org/10.1126/science.236.4804.942.

Audet, P., Bostock, M.G., Christensen, N.I., Peacock, S.M., 2009. Seismic evidence for overpressured subducted oceanic crust and megathrust fault sealing. Nature 457 (7225), 76–78. http://dx.doi.org/10.1038/nature07650.

Bartlow, N.M., Miyazaki, S., Bradley, A.M., Segall, P., 2011. Space-time correlation of slip and tremor during the 2009 Cascadia slow slip event. Geophys. Res. Lett. 38, L18309. http://dx.doi.org/10.1029/2011GL048714.

Bostock, M.G., Hyndman, R.D., Rondenay, S., Peacock, S.M., 2002. An inverted continental Moho and serpentinization of the forearc mantle. Nature 417, 536–538. http://dx.doi.org/10.1038/417536a.

Brown, J.R., Beroza, G.C., Ide, S., Ohta, K., Shelly, D.R., Schwartz, S.Y., Rabbel, W., Thorwart, M., Kao, H., 2009. Deep low-frequency earthquakes in tremor localize to the plate interface in multiple subduction zones. Geophys. Res. Lett. 36, L19306. http://dx.doi.org/10.1029/2009GL040027.

Brudzinski, M.R., Allen, R.M., 2007. Segmentation in episodic tremor and slip all along Cascadia. Geology 35, 907–910. http://dx.doi.org/10.1130/G23740A.1.

Burgette, R.J., Weldon II, R.J., Schmidt, D.A., 2009. Interseismic uplift rates for western Oregon and along-strike variation in locking on the Cascadia subduction zone. J. Geophys. Res. 114, B01408. http://dx.doi.org/10.1029/2008JB005679.

Chapman, J.S., Melbourne, T.I., 2009. Future Cascadia megathrust rupture delineated by episodic tremor and slip. Geophys. Res. Lett. 36, L22301. http://dx.doi.org/10.1029/2009GL040465.

Chen, W.-P., Molnar, P., 1983. Focal depths of intracontinental and intraplate earthquakes and their implications for the thermal and mechanical properties of the lithosphere. J. Geophys. Res. 88, 4183–4214. http://dx.doi.org/10.1029/JB088iB05p04183.

Colella, H.V., Dieterich, J.H., Richards-Dinger, K., 2013. Spatial and temporal patterns of simulated slow slip events on the Cascadia megathrust. Geophys. Res. Lett. 40, 5101–5107. http://dx.doi.org/10.1002/grl.50984.

Dragert, H., Wang, K., 2011. Temporal evolution of an episodic tremor and slip event along the northern Cascadia margin. J. Geophys. Res. 116, B12406. http://dx.doi.org/10.1029/2011JB008609.1.

Dragert, G., Wang, K., James, T.S., 2001. A silent slip event on the deeper Cascadia subduction interface. Science 292, 1525–1528. http://dx.doi.org/10.1126/science.1060152.

Gao, H., Humphreys, E.D., Yao, H., van der Hilst, R.D., 2011. Crust and lithosphere structure of the northwestern U.S. with ambient noise tomography: terrane accretion and Cascade arc development. Earth Planet. Sci. Lett. 304, 202–211. http://dx.doi.org/10.1016/j.epsl.2011.01.033.

Ghosh, A., Vidale, J.E., Sweet, J.R., Creager, K.C., Wech, A.G., Houston, H., 2010. Tremor bands sweep Cascadia. Geophys. Res. Lett. 37, L08301. http://dx.doi.org/10.1029/2009GL042301.

Goldfinger, C., Nelson, C.H., Johnson, J.E., 2003. Holocene earthquake records from the Cascadia subduction zone and northern San Andreas Fault based on precise dating of offshore turbidites. Annu. Rev. Earth Planet. Sci. 31, 555–577. http://dx.doi.org/10.1146/annurev.earth.31.100901.141246.

Holtkamp, S., Brudzinski, M.R., 2010. Determination of slow slip episodes and strain accumulation along the Cascadia margin. J. Geophys. Res. 115, B00A17. http://dx.doi.org/10.1029/2008JB006058.

Hyndman, R.D., Wang, K., 1995. The rupture zone of Cascadia great earthquakes from current deformation and the thermal regime. J. Geophys. Res. 100 (B11), 22,133–22,154. http://dx.doi.org/10.1029/95JB01970.

Ide, S., Beroza, G.C., Shelly, D.R., Uchide, T., 2007. A scaling law for slow earthquakes. Nature 447, 76–79. http://dx.doi.org/10.1038/nature05780.

Mazzotti, S., Lambert, A., Courtier, N., Nykolaishen, L., Dragert, H., 2007. Crustal uplift and sea level rise in northern Cascadia from GPS, absolute gravity, and tide gauge data. Geophys. Res. Lett. 34, L15306. http://dx.doi.org/10.1029/2007GL030283.

McCaffrey, R., Long, M.D., Goldfinger, C., Zwick, P.C., Nabelek, J.L., Johnson, C.K., Smith, C., 2000. Rotation and plate locking at the Southern Cascadia Subduction Zone. Geophys. Res. Lett. 27 (19), 3117. http://dx.doi.org/10.1029/2000GL011768.

McCaffrey, R., King, R.W., Payne, S.J., Lancaster, M., 2013. Active tectonics of northwestern U.S. inferred from GPS-derived surface velocities. J. Geophys. Res. Solid Earth 118, 709–723. http://dx.doi.org/10.1029/2012JB009473.

McCrory, P.A., Blair, J.L., Oppenheimer, D.H., Walter, S.R., 2004. Depth to the Juan de Fuca slab beneath the Cascadia subduction margin: a 3-D model for sorting earthquakes. Data Ser. 91. U.S. Geol. Surv., Reston, Va.

Nedimovic, M.R., Hyndman, R.D., Ramachandran, K., Spence, G.D., 2003. Reflection signature of seismic and aseismic slip on the northern Cascadia subduction interface. Nature 424, 416–420. http://dx.doi.org/10.1038/nature01840. http://dx.doi.org/10.1038/nature01828.

Nicholson, T., Bostock, M.G., Cassidy, J.F., 2005. New constraints on subduction zone structure in northern Cascadia. Geophys. J. Int. 161, 849–859.

Peacock, S.M., Christensen, N.I., Bostock, M.G., Audet, P., 2011. High pore pressures and porosity at 35 km depth in the Cascadia subduction zone. Geology 39 (5), 471–474. http://dx.doi.org/10.1130/G31649.1.

Petersen, M.D., Moschetti, M.P., Powers, P.M., Mueller, C.S., Haller, K.M., Frankel, A.D., Zeng, Y., Rezaeian, S., Harmsen, S.C., Boyd, O.S., Field, N., Chen, R., Rukstales, K.S., Luco, N., Wheeler, R.L., Williams, R.A., Olsen, A.H., 2014. Documentation for the 2014 update of the United States national seismic hazard maps. U.S. Geological Survey open-file report 2014–1091, 243 p. http://dx.doi.org/10.3133/ofr20141091.

Pollitz, F.F., Bürgmann, R., Segall, P., 1998. Joint estimation of afterslip rate and postseismic relaxation following the 1989 Loma Prieta earthquake. J. Geophys. Res. 103 (B11), 26975–26992. http://dx.doi.org/10.1029/98JB01554.

Rogers, G., Dragert, H., 2003. Episodic tremor and slip on the Cascadia subduction zone: the chatter of silent slip. Science 300, 1942–1943. http://dx.doi.org/10.1126/science.1084783.

Savage, J.C., Svarc, J.L., Prescott, W.H., Murray, M.H., 2000. Deformation across the forearc of the Cascadia subduction zone at Cape Blanco, Oregon. J. Geophys. Res. 105 (B2), 3095–3102. http://dx.doi.org/10.1029/1999JB900392.

Schmidt, D.A., Gao, H., 2010. Source parameters and time-dependent slip distributions of slow slip events on the Cascadia subduction zone from 1998 to 2008. J. Geophys. Res. 115, B00A18. http://dx.doi.org/10.1029/2008JB006045.

Segall, P., Rubin, A.M., Bradley, A.M., Rice, J.R., 2010. Dilatant strengthening as a mechanism for slow slip events. J. Geophys. Res. 115, B12305. http://dx.doi.org/10.1029/2010JB007449.

Thomas, A.L., 1993. Poly3d: A three-dimensional, polygonal element, displacement discontinuity boundary element computer program with applications to fractures, faults, and cavities in the Earths crust. Stanford Univ, Stanford, Calif., 69 pp.

Verdonck, D., 2005. An inverse dislocation model of surface deformation in western Washington. Tectonophysics 395 (3–4), 179–191. http://dx.doi.org/10.1016/j.tecto.2004.09.010.

Wang, K., He, J., Dragert, H., James, T.S., 2001. Three-dimensional viscoelastic interseismic deformation model for the Cascadia subduction zone. Earth Planets Space 53 (4), 295–306. http://dx.doi.org/10.1186/BF03352386.

Wang, K., Wells, R., Mazzotti, S., Hyndman, R.D., Sagiya, T., 2003. A revised dislocation model of interseismic deformation of the Cascadia subduction zone. J. Geophys. Res. 108 (B1), 2026. http://dx.doi.org/10.1029/2001JB001227.

Wang, K., Dragert, H., Kao, H., Roeloffs, E., 2008. Characterizing an "uncharacteristic" ETS event in northern Cascadia. Geophys. Res. Lett. 35, L15303. http://dx.doi.org/10.1029/2008GL034415.

Wech, A.G., 2010. Interactive tremor monitoring. Seismol. Res. Lett. 81 (4), 664–669.

Wech, A.G., Creager, K.C., 2011. A continuum of stress, strength and slip in the Cascadia subduction zone. Nat. Geosci. 4 (9), 624–628. http://dx.doi.org/10.1038/ngeo1215.

Wech, A.G., Creager, K.C., Melbourne, T.I., 2009. Seismic and geodetic constraints on Cascadia slow slip. J. Geophys. Res. 114, B10316. http://dx.doi.org/10.1029/2008JB006090.

Wells, R.E., Simpson, R.W., 2001. Northward migration of the Cascadia forearc in the northwestern US and implications for subduction deformation. Earth Planets Space 53 (4), 275–283.

Williams, C.A., Wallace, L.M., 2015. Effects of material property variations on slip estimates for subduction interface slow-slip events. Geophys. Res. Lett. 42, 1113–1121. http://dx.doi.org/10.1002/2014GL062505.

Wyatt, F.K., 1989. Displacement of surface monuments: vertical motion. J. Geophys. Res. 94 (B2), 1655–1664. http://dx.doi.org/10.1029/JB094iB02p01655.